SYNTHESIS AND CHARACTERIZATION OF UV DETECTORS BASED ON ZnO AND ALDOPED ZnO NANORODS

[1]HUSSEIN ABDULLAH ALSHAMARTI, [2]AREF SALEH BARON, [3]ALI ABID ABOJASSIM

[1,2,3]Department of Physics, Faculty of Science, University of Kufa, Iraq
E-mail: [1]husseina.alshemirti@uokufa.edu.iq, [2]arif.aljuburi@uokufa.edu.iq, [3]ali.alhameedawi@uokufa.edu.iq

Abstract - ZnO and Al-doped ZnO nanorods (NRs) were synthesis to fabricated UV detector devices deposited on N-type Si, Two methods used to synthesis sol-gel and Chemical bath deposition (CBD). The crystalline properties indicated shifting in the peaks of XRD patterns of Al-doped ZnO relative to ZnO patterns. The detection of UV radiation was apparent through the results of the UV detector parameters. The doping process by Al improved the characterization of photo-detector devices where the external quantum efficiency (EQE) of enhancement from 67.94% to 135.89% at wavelength 365nm and reached to 901.8% at wavelength 385 nm.

Keywords - ZnO nanorod, Al-doped, Sol gel, Chemical Bath deposition, UV-detector

I. INTRODUCTION

ZnO is one of the famous components of the II-VI group which used in semiconductors in difference optical applications such as solar cells, optical detectors and light emitting diode etc. There are many properties of ZnO is this useful is a which used as Zinc Oxide (ZnO) is one attractive oxide materials, because of its wide resistivity range (10^{-4} – 10^{12} Ω·cm), direct wide energy gap is 3.37 eV and large exciting binding energy a 60 meV, at temperature 300 K [1-5] . ZnO nanostructure can be get it by different shapes depend on quantum confinement dimensional, for one dimensional there are, nanorods, nanowire, and nanotube etc. Also that these structures can be controlling it by confidence prepared methods, like sol–gel method[5], evaporating methods (which include solid-liquid, solid-solid)[6], laser ablation method[7], hydrothermal method[8] and chemical bath deposition[9], etc. The chemical bath method is a widely used because it easy using, not used high temperature or vacuum system and low coast.

Often used seed layer from ZnO to ensure growth of the ZnO NRs, on the other hand to improve the properties of ZnO nanostructures by doping a different chemical elements such as Na[10], Sn [11], Fe [12], Mn[13], Mg[14], and Al[15, 16] into ZnO structures. Among them, Al-doped ZnO nanorods are capable of reaching the highest conductivity without deterioration in optical transmission and crystallinity, and thus have been regarded as a potential alternative to the most accepted transparent conductive material.
In this paper, we fabricated ZnO NRs by used to methods, sol-gel for seed layer ZnO and grown ZnO nanorods by CBD method. Two types ZnO devices were fabricated, pure ZnO and ZnO doped Al devices, as UV detectors. Finally, we comparing between these devices from parameters of UV detectors.

II. EXPERERIMENTAL PROCEDURE

ZnO nanorods (NRs) prepared by two steps: sol-gel and CBD methods were it prepare on n-type silicon as substrates. Firstly, the cleaning stage which include cleaned the silicon substrate by ultrasonically with propanol, acetone and deionized water. Secondly, 0.01 M of Zn $(CH_3COO)_2 .2H_2O$) (Zinc acetate dihydrate) was dissolve in absolute ethanol(99%), under vigorous stirring at 55°C about 3 hours. The solution was transparent and homogeneous after this time. Then, the resultant solution was spin-coated on the n-type silicon substrate with a speed of 2000 rpm for 20 s at room temperature. The resultant film have a homogeneous seed layer of the ZnO and dried it at (110 ± 5)°C about 10-12 mines to dispose of the organic residuals. Repeat this process for 6 times, then annealed the samples at (400 ±10) °C for 2 h by using a controlling furnace. The CBD method was used to prepare the ZnO nanorod and Al-doped ZnO (AZO). In this method the substrate was putting vertically in the tow closed beakers which consist of aqueous solution. The first beaker includes aqueous solution from Zn $(NO_3)_2.6H_2O$ (Zinc nitrate hexahydrate) in concentrations 0.01M and 0.01M hexamethylenetetramine $C_6H_{12}N_4$ to prepare the ZnO nanorod and classified as simple S1. The second beaker had same solution and reaction with 5% of Aluminum nitrate $Al(NO_3)_3.9H_2O$ to prepare Al-doped ZnO which classified as simple S2 . Tow beakers were treated in temperature 90°C for 2h. Finally, the samples S1 and S2 were washed by distilled water and annealed at 400°C for 1h.

III. RESULTS AND DISCUSSION

The results of this paper include XR diffraction, FESEM, and values of UV detector device. Figure 1 shows the XRD patterns of ZnO (black line) and Al-ZnO (red line) are deposited on the N-type silicon substrate for named S1 and S2 samples, respectively.

The mean peaks for this sample appeared at positions 31.8º, 347.2º, 36.24º, which have miller indices (1 0 0), (0 0 2), (1 0 1), respectively. These are results corresponding with the ZnO hexagonal wurtzite-type structure and with (Joint Committee on Powder Diffraction Standard (JCPDS) card No. 89-1397). By comparing the results, we find that there is a very agreement between the peaks of the two figures, where it appears that the doping peaks are more severe and the intensity exceeds the ZnO sample.

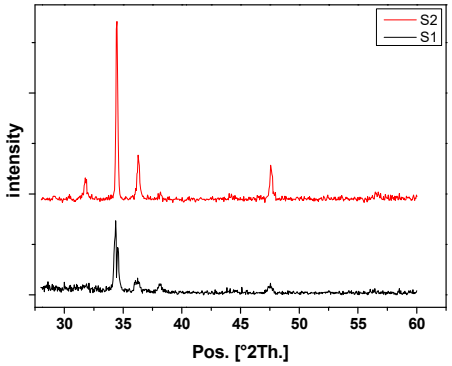

Figure 1: XRD patterns of pure ZnO deposited on the Si substrate

The Field Emission Scanning Electron Microscope (FESEM) investigated the surface morphology images of the grown ZnO nanorods (sample S1) deposited on the n-Si substrate as shown in Figure 2a and Figure 2c.

On other hand, the surface morphology of Al-doped ZnO nanorods of sample S2 were as shown in Figure 2b and Figure 2d. A small changing in hexagonal shape of rods with doping of Al was noticed.

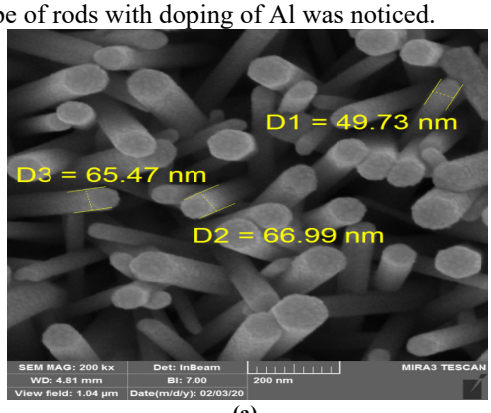

(a)

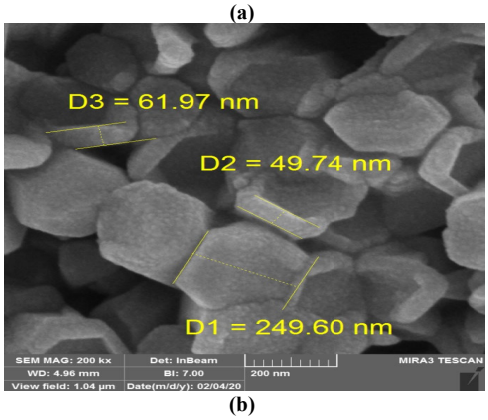

(b)

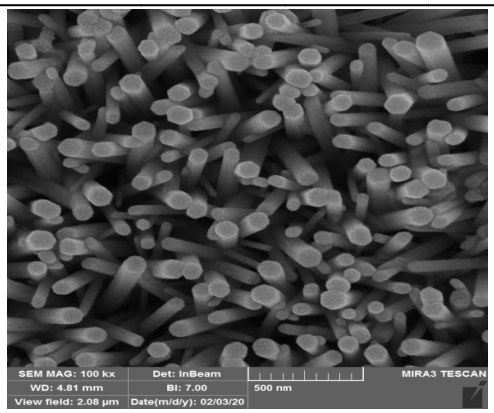

(c)

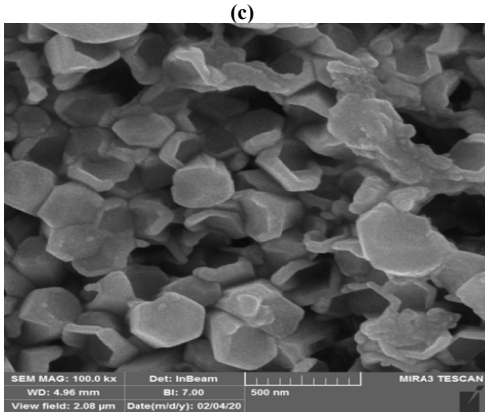

(d)

Figure 2: FESEM image of pure ZnO nanorods deposited on the N-Si substrate with scales a) S1 (scale: 200 nm), b) S2 (scale: 200 nm), c) S1 (scale: 500 nm) and d) S2 (scale: 500 nm),

The final result corresponding the UV detector device which illuminated it's by two different light incident wavelengths (365 nm and 385 nm) having a same power (45 $\mu W.cm^{-1}$). Figure 3 explain the I-V characterization which included the dark and light (365 and 385 nm wavelengths) current state for tow sample S1and S2 detectors, respectively.

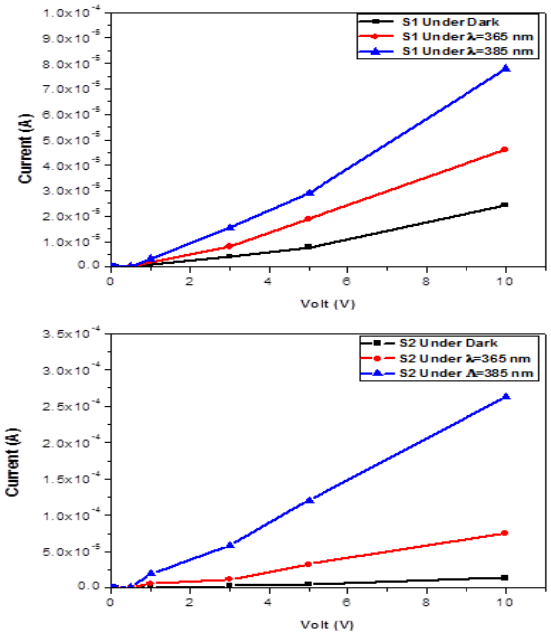

Figure 3: I-V characterization of S1-Ph and S2-Ph devices.

The photocurrent is resulting due to by generated a excitons when the photon strike the photodetector device, might be separated to the electron-hole pairs which produced by the interaction the exactions and the trap centers in the device which that increases with doping [17] and this appeared clearly in the sample S2. The dark current for sample S1 was reached to $2x10^{-5}$ A as a high value, after illuminating by 365nm the photocurrent increased to $4x10^{-5}$ A. While increased to $8x10^{-5}$ A when illuminated by wavelength 385nm. The photocurrent for sample S2 jumped from $1x10^{-5}$ A; for dark current; to $7.5x10^{-5}$ A and $2.75x10^{-4}$ A when illuminating by wavelengths 365nm , 365nm, respectively.

Figure 4 showed the photoresponse of sample S1 fabricated device under 365 nm and 385 nm wavelengths. The current is rising to the saturation state when the incident light was switched on and then decreased when it was switched off. The responsively of device appear clearly where the value of current changing from $4*10^{-6}$ A for I_{dark} to $8*10^{-6}$A for I_{light} to one cycle. While the difference between current dark and current light appear more clearly when the illumination light wavelength is 385nm, where $I_{dark} = 4*10^{-6}$ A and $I_{light} = 1.6*10^{-5}$A.

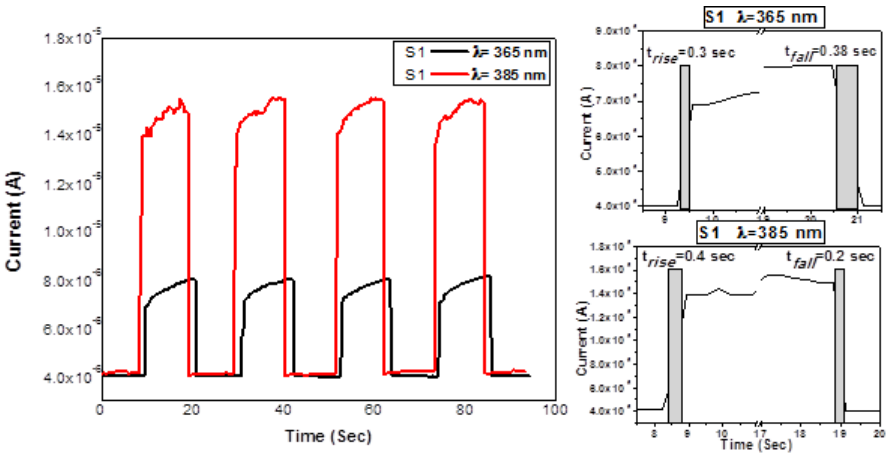

Figure4: The photoresponse and current-time relation of S1 device under 365 nm and 385 nm wavelengths.

The response time of a UV detector device is determined by two parameters: rise time t_{rise} which define as the value of photocurrent to growth from 10% to 90% of the greatest value and vice versa for fall time t_{fall} [18]. The rise time and fall time appear rapidly response for two light illuminated, t_{rise}=0.3s, t_{fall} =0.38s and trise=0.4s, t_{fall} =0.2s for wavelengths λ=365 nm and λ=385nm, respectively, see figure(3).

The photoresponse of S2-Ph fabricated device appear more clearly under 365 nm and 385 nm wavelengths .The $I_{dark} = 2*10^{-6}$ A and I_{light} $1*10^{-5}$A when the illuminated light wavelength is 365 nm .In addition the $I_{dark} = 2*10^{-6}$ A and I_{light} $5.8*10^{-5}$A when the illuminated light 385 nm. This increase is due to the doping process. Whither this doping led to the formation of internal levels in the energy gap, the transmission of electron-hole pairs within the energy gap increased[19]. The response times recorded were: t_{rise}=0.4s, t_{fall} =0.22s and t_{rise}=0.5s, t_{fall} =0.2s for wavelengths 365 nm and 385nm respectively, see figure(4).

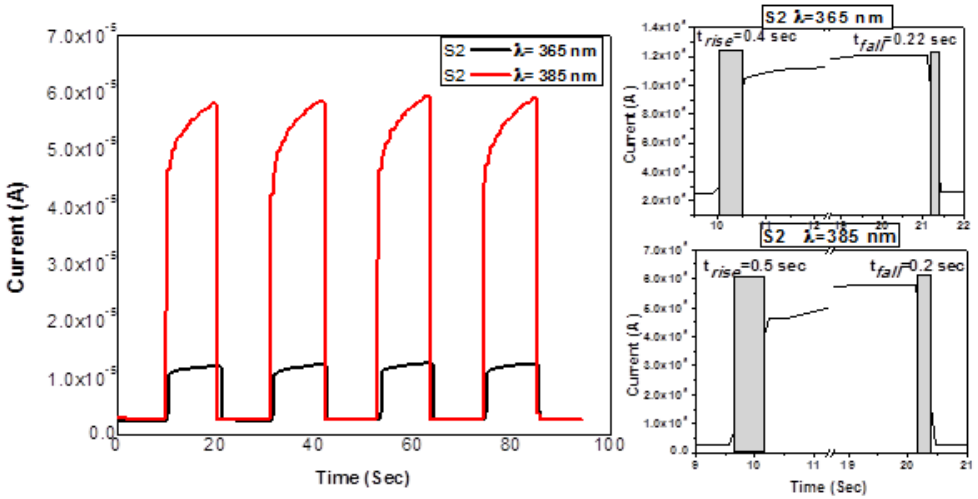

Figure 4: The photoresponse and current-time relation of S2 device under 365 nm and 385 nm wavelengths.

The UV -detector parameters can be computation by depend on some relations,

$$R = \frac{I_{light} - I_{dark}}{PA}$$

Where R epitomize the UV responsivity of UV -detector, P the power of the incident light (W), and A is represented the effectual area of the UV -detector (cm^2). The Photo responsivity R increasing when the wavelength of incident light increase where the value change from 0.2 to 0.6 $A.W^{-1}$ for 365 and 385 nm wavelengths respectively. In the same time the Photo responsivity R increasing with the doping processing by Al-doped attributed to extra free carrier. Also that this facilitates the mobility of charge carriers due to the formation of internal energy levels within the energy gap [20]. These results appear clearly when calculated the external quantum efficiency (EQE) which represent number of electrons resulted per incident light[21]. The doping is processing improving the EQE of UV detector, where enhancement EQE from 67.94% (without Al-doped) to 135.89% (with Al-doped) at wavelength 365nm. A maximum EQE reached to 901.8% at 385 nm when doped UV detector device by Al. At the same time, the sensitivity increases for the same reasons that passed previously as shown in table(1), depending on wavelength of incident light and Al-doped.

	Wavelength nm	t_{rise} (s)	t_{fall} (s)	RA.W^{-1}	Q %	S %
ZnO pure	365	0.3	0.38	0.2	67.94	100
	385	0.4	0.2	0.6	193.24	300
Al-ZnO	365	0.4	0.22	0.4	135.89	400
	385	0.5	0.2	2.8	901.8	2800

Table 1: Photo-detector parameters of S2 and S2 devices

IV. CONCLUSION

Implemented with any type of adder to further improve the speed. Using Binary to Excess-1 Converter (BEC) instead of RCA in the regular CSLA we can achieve lower area and power consumption. The main advantage of this BEC logic comes from the lesser number of logic gates than the Full Adder (FA) structure.is therefore, low area, low power, simple and efficient A to excess-1 code converters (BEC) to improve the speed of addition. This logic can be for VLSI hardware implementation. In this paper, UV detector devices were fabricated depending on ZnO NRs (ZnO nanorods) and Al-doped ZnO , have been successfully prepared by sol-gel and CBD methods, were used n-type silicon as substrates. Their physical and photo electronic properties were investigated. XRD analysis shows shifting in the peaks of Al-doped ZnO pattern's compared to ZnO patterns. The results of the UV detector parameters indicated that the effect of the wavelength improved those results when increasing it for wavelengths 365nm to 385nm in the UV region, Also that these results are improved when the ZnO was doped.

REFERENCES

[1] Ubale, A. and V. Deshpande, Effect of manganese inclusion on structural, optical and electrical properties of ZnO thin films. Journal of alloys and compounds, 2010. 500(1): p. 138-143.

[2] Dutta, S., et al., Role of defects in tailoring structural, electrical and optical properties of ZnO. Progress in Materials Science, 2009. 54(1): p. 89-136.

[3] Pourshaban, E., H. Abdizadeh, and M.R. Golobostanfard, ZnO nanorods array synthesized by chemical bath deposition: effect of seed layer sol concentration. Procedia Materials Science, 2015. 11: p. 352-358.

[4] Kumar, V., et al., Rare earth doped zinc oxide nanophosphor powder: a future material for solid state lighting and solar cells. Acs Photonics, 2017. 4(11): p. 2613-2637.

[5] Dev, A., A. Elshaer, and T. Voss, Optical applications of ZnO nanowires. IEEE Journal of Selected Topics in Quantum Electronics, 2010. 17(4): p. 896-906.

[6] Qiu, M., et al., Growth and properties of ZnO nanorod and nanonails by thermal evaporation. Applied Surface Science, 2009. 255(7): p. 3972-3976.

[7] Gupta, V., et al., Optical phonon modes in ZnO nanorods on Si prepared by pulsed laser deposition. Journal of crystal growth, 2006. 287(1): p. 39-43.

[8] Zhao, W., et al., Room Temperature Ferromagnetic and Optical Properties of Chrome Doped ZnS Nanorods Prepared by Hydrothermal Method. Journal of Nanomaterials, 2017. 2017.

[9] Gurav, K., et al., Controlled crystallite orientation in ZnO nanorods prepared by chemical bath deposition: Effect of H2O2. Journal of alloys and compounds, 2011. 509(29): p. 7723-7728.

[10] Ye, Z., et al., Na-doped ZnO nanorods fabricated by chemical vapor deposition and their optoelectrical properties. Journal of alloys and compounds, 2017. 690: p. 189-194.

[11] Wu, C., et al., Synthesis of Sn-doped ZnO nanorods and their photocatalytic properties. Materials Research Bulletin, 2011. 46(7): p. 1107-1112.

[12] Kaur, J., et al., Anionic polymerization in Co and Fe doped ZnO: nanorods, magnetism and photoactivity. Current Applied Physics, 2014. 14(5): p. 749-756.

[13] Alshamarti, H.A. and A.H.O. Alkhayatt, Enhancement characterization of the MSM detector based on Mn doped-ZnO NRS synthesized by microwave assisted chemical bath deposition. Materials Science in Semiconductor Processing, 2020. 114: p. 105068.

[14] Hameed, H.A., J. Hassan, and H. Saadon, Fabrication and Enhancement UV Photodiode Based on Mg-Doped ZnO Nanorods Films. Iraqi Journal of Science, 2019: p. 7-16.

[15] Navaneethan, M., et al., Influence of Al doping on the structural, morphological, optical, and gas sensing properties of ZnO nanorods. Journal of alloys and compounds, 2017. 698: p. 555-564.

[16] Shrisha, B., et al., Hydrothermal growth and characterization of Al-doped ZnO nanorods. Materials Today: Proceedings, 2016. 3(6): p. 1693-1701.

[17] Chey, C.O., et al., Fast piezoresistive sensor and UV photodetector based on Mn-doped ZnO nanorods. physica

status solidi (RRL)–Rapid Research Letters, 2015. 9(1): p. 87-91.

[18] Baron, A.S., S.J. Kasim, and A.H. Omran, Fabrication of a Solar Cells by Organic-Inorganic Hybrid Perovskites. Indian Journal of Public Health Research & Development, 2018. 9(12): p. 1276-1281.

[19] Bai, Z., et al., Self-powered ultraviolet photodetectors based on selectively grown ZnO nanowire arrays with thermal tuning performance. Physical Chemistry Chemical Physics, 2014. 16(20): p. 9525-9529.

[20] Khayatian, A., et al., Diameter-controlled synthesis of ZnO nanorods on Fe-doped ZnO seed layer and enhanced photodetection performance. Materials Research Bulletin, 2017. 94: p. 77-84.

[21] Prabhakar, R.R., et al., Efficient multispectral photodetection using Mn doped ZnO nanowires. Journal of Materials Chemistry, 2012. 22(19): p. 9678-9683.

★★★